

Received January 2, 2021, accepted January 28, 2021, date of publication February 1, 2021, date of current version February 10, 2021.

Digital Object Identifier 10.1109/ACCESS.2021.3056148

Signal Pre-Equalization in a Silicon Photomultiplier-Based Optical OFDM System

CUIWEI HE^{ID}, ZUBAIR AHMED^{ID}, AND STEVE COLLINS^{ID}, (Member, IEEE)

Department of Engineering Science, University of Oxford, Oxford OX1 3PJ, U.K.

Corresponding author: Cuiwei He (cuiwei.he@eng.ox.ac.uk)

This work was supported in part by the Punjab Educational Endowment Fund, Pakistan, and in part by the U.K. Engineering and Physical Sciences Research Council (EPSRC) under Grant EP/R00689X/1. The research materials supporting this publication can be accessed by contacting steve.collins@eng.ox.ac.uk.

ABSTRACT In this article, the performance of a new time domain signal pre-equalization method for use with optical orthogonal frequency division multiplexing (OFDM) and a silicon photomultiplier (SiPM) based receiver is studied. A SiPM contains a large array of microcells and each microcell is able to detect single photons. Therefore, a SiPM can be used to create arguably the most sensitive optical receiver, which can detect light intensity signals by counting the number of arriving photons within each signal sampling period. However, each photon detection triggers an avalanche-and-quenching process and the related microcell becomes inactive for a recovery time of several nanoseconds. Consequently, any photons arriving during this period cannot be detected. This effect can cause a non-linear distortion of the received signal and, when the OFDM sampling period is short, also introduces interference between signal samples. In this article, a new signal pre-equalization method is specifically designed to compensate for the impact of the finite recovery time. In this method, the number of active microcells during the transmission of each OFDM signal sample is first estimated. Then, the amplitude of the time domain signal sample is pre-adjusted based on the predicted fraction of microcells that are active. Using this approach, the negative impacts of the recovery time of the microcells are significantly reduced. The results that are presented show that when this new form of pre-equalization is used the bit error rate (BER) performance of the system is improved for a wide range of irradiance levels.

INDEX TERMS SiPM, SPAD, nonlinearity, pre-equalization, optical OFDM.

I. INTRODUCTION

Indoor visible light communication (VLC) is emerging as a cutting-edge technology for high-speed wireless data transmission [1]–[5], whose achievable data rate depends on the sensitivity of the optical receiver [6]. Consequently, the receiver is a critical component of any VLC system and one promising approach to creating a very sensitive VLC receiver is to use a silicon photo-multiplier (SiPM). These devices contain an array of microcells that can detect single photons. In each microcell, which is also known as a single photon avalanche diode (SPAD), an avalanche photodiode (APD) is biased above its breakdown voltage and placed in series with a quenching device. A single photon arriving on a microcell can then trigger an avalanche-and-quenching process. This process generates an output pulse and the associated photon can therefore be counted [7].

The associate editor coordinating the review of this manuscript and approving it for publication was Qunbi Zhuge^{ID}.

However, the quenching process means that a microcell needs a recovery period after it has detected a photon. Any photons arriving during this recovery period cannot be detected and this causes a nonlinear response of the receiver which limits the performance of the overall system [8], [9].

In the previous studies of SiPM based receivers in optical wireless communications, on-off keying (OOK) was used as the modulation method [8], [10], [11]. Despite the nonlinear response of the SiPM detector, a transmission data rate of 3.45 Gbps has been demonstrated [10]. More importantly, when the transmission data rate is below 1 Gbps, the SiPM detector has been shown to be more sensitive than other types of receivers [8]. Moreover, many types of commercial off-the-shelf SiPM are now available from companies including Hamamatsu, On Semiconductor and Ketek.

Currently, there is significant interest in using optical orthogonal frequency division multiplexing (OFDM) in VLC [12], [13]. This is because OFDM possesses several advantages. For example, in OFDM, the addition and removal

of the cyclic prefix (CP) can completely eliminate interference between different OFDM symbols. Consequently, each OFDM symbol can be equalized individually using a set of single-tap equalizers in the frequency domain [12]. This is potentially a very important advantage of using OFDM in high data rate VLC systems. However, when a SiPM is used with OFDM modulation, the system encounters some unique challenges. First, OFDM signals normally have high peak-to-average power ratios. The nonlinear response of the SiPM may then distort any OFDM signal samples which are associated with high instantaneous optical power. Second, when the transmission data rates are high, the recovery period of the microcells may span multiple signal samples. When combined with the high peak signal power in OFDM this will result in a new form of inter-symbol interference (ISI). Although several studies of the use of a SPAD array with OFDM modulation have been published [14]–[16], the negative impact of the SPAD's nonlinearity have not been thoroughly investigated. For example, in [15], [16], the sampling periods were set to be significantly longer than the recovery period and the nonlinearity of the SPAD array only affected individual signal samples. As a result, the demonstrated data rates were only 1 Kbps and 1 Mbps [15], [16]. In [14], although the maximum simulated transmission data rate was 100 Mbps, the influence of the SPAD's nonlinearity was not investigated.

In [17], [18], a linear post-equalization method was studied to mitigate the interference caused by the recovery period based on the photon arrival time information. However, this approach is complex and the inactive periods of individual SPADs were tracked. Consequently, this method is not applicable to any receiver containing the commercial SiPMs which have a single shared output. In [19], we investigated the performance of a commercial SiPM when used with OFDM and predicted that using conventional frequency domain single-tap equalizers a data rate of 187 Mbps is achievable. However, when the sampling period of the transmitted signal is further reduced, the system would confront a second type of interference. In particular, when the data rate is above several Mbps, the sampling period of the transmitted signal is much shorter than the recovery time of the microcell [19]. This causes a unique form of signal interference which would result in data detection failures when no equalization is used [19]. Moreover, when the transmission data rate is further increased to several hundred Mbps or above, the sampling period of the signal needs to be shorter than the width of the output pulse generated from the avalanche-and-quenching process. In this case, the bandlimited channel creates a conventional form of interference [20]. These two forms of interference have different origins and therefore are expected to be resolved using different equalization techniques. Conventional post-equalization is commonly used to compensate for interference arising from the channels limited bandwidth. Therefore, ideally pre-equalization at the transmitter should be used to compensate for any interference caused by the recovery period.

In this article a new pre-equalization method, which is specially designed to mitigate the interference caused by the recovery period of SiPM microcells is described and its performance with optical OFDM modulation is simulated. In this method, the amplitudes of the transmitted signal samples are pre-adjusted based on the estimated fraction of active microcells within each sampling period. One advantage of this approach is that conventional post-equalization remains available to mitigate any ISI caused by a band limited channel. It is shown that the negative impact of the recovery time can be significantly reduced using this new pre-equalization method. In addition, simulation results are presented which show the advantages of using a SiPM with larger number of microcells and hence higher maximum count rate.

The rest of the paper is structured as follows. Section-II summarizes the key characteristics of the SiPMs that are considered and how the characteristics can affect the achievable data rate. In Section-III, the Monte Carlo model which is used to simulate the photon counting process is explained. Using this model, in Section-IV, simulation trials are used to explain the origins of the SiPM detector's nonlinearity and how it causes interference between different signal samples at high data rate scenarios. The new pre-equalization method used to compensate for this type of interferences is described in Section-V. Section-VI shows the overall SiPM based optical OFDM system. The simulated BER results are presented in Section-VII. Finally, Section-VIII concludes the paper.

II. SiPM CHARACTERISTICS

In this section, the main characteristics of SiPMs which affect the achievable data rate are discussed. Two different SiPMs from the On Semiconductor J series, the SiPM 30035 and SiPM 60035, are considered in this article and their key parameters are listed in Table-1. In the following, the influences of the microcell's recovery time and the output pulse width are discussed in detail. Although many SiPM parameters, such as the after pulsing probability, the crosstalk probability, can also affect the overall transmission, their impacts are relatively small and will be analyzed in detail in future experiments.

One important SiPM parameter is the recovery time of the microcells. After detecting a photon a microcell in a SiPM needs a period to recover and any photons that are incident on the microcell within the recovery period cannot be counted. Consequently, at higher photon fluxes, the number of detected photons is not linearly related to the intensity of the light falling on the SiPM. The negative impacts of this nonlinearity on the overall system are related to the data rate. Table-1 shows that the recovery period for the SiPM 30035 is 45 ns and that for the SiPM 60035 is 50 ns. When the data rate is only a few Mbps or below, the sampling period of the transmitted signal is typically much greater than the microcell's recovery period. In this case, the nonlinearity only affects the amplitude of individual signal samples associated with high instantaneous optical power and this situation has been considered in [16]. When the transmission data rate

TABLE 1. SiPM Parameters (30035 & 60035) from data sheets [21].

SiPM model	30035	60035
Active area	$3.07 \times 3.07 \text{ mm}^2$	$6.07 \times 6.07 \text{ mm}^2$
Number of microcells, N_{cells}	5676	22292
Fill factor	75%	75%
Photon detection efficiency (405 nm)	38%	38%
Dark count rate	50 KHz/mm ²	50 KHz/mm ²
Recovery time, τ	45 ns	50 ns
Fast output pulse width	1.5 ns	3 ns
After pulsing probability	0.75 %	0.75 %
Crosstalk probability	8 %	8 %

is increased by reducing the signal's sampling period, this nonlinearity starts to affect multiple signal samples and cause interference between them. This type of interference can severely degrade the overall performance of the transmission. Also, it has unique features which makes it very different from the usual ISI.

In VLC systems ISI is usually caused by overlap between symbols caused by the limited channel bandwidth. When a SiPM is used in a VLC receiver one contribution to this form of ISI will be the finite duration of its output pulses. The J-Series SiPMs from On Semiconductor can be purchased on an evaluation board which provides both a standard output and a capacitively coupled fast output. As listed in Table-1, the pulse width of the fast output is 1.5 ns for SiPM 30035 and 3 ns for SiPM 60035. These parameters suggest that the more usual type of ISI is expected when the symbol time is a few ns. This common form of interference can be mitigated using conventional equalizers, including the post-equalizers often used with OFDM. In this article, the minimum sampling period considered is 5 ns, which is longer than the pulse width and therefore the usual type of ISI is not considered. The influence of this form of ISI on the overall achievable data rate will be determined by future experiments.

III. SIMULATION MODEL

This section introduces a Monte Carlo model which is used to simulate the photon counting process based on the received light intensity. In this model, an inverse cumulative distribution function (CDF) method is used to simulate the arrival time of individual photons, which follow an exponential distribution so that the number of photons arriving within a constant time period is a Poisson variable. Moreover, by taking the microcell's recovery period into account, the number of detected photons can be simulated.

A. STATISTICAL MODEL

During the transmission of the k th signal sample, the number of photons, v_k , arriving at each microcell can be accurately modelled using a Poisson distribution. This distribution has a probability mass function (PMF) given by

$$P(v_k = j) = \frac{\mu_k^j e^{-\mu_k}}{j!} \quad (1)$$

where μ_k is the average number of photons arriving during the k th sample. This is related to the instantaneous optical power received by the SiPM, $r_{\text{opt}}(t)$, by

$$\mu_k = \frac{\alpha_{\text{PDE}}}{N_{\text{cells}} E_p} \int_{t_k}^{t_k + T_s} r_{\text{opt}}(t) dt \quad (2)$$

In (2), $\int_{t_k}^{t_k + T_s} r_{\text{opt}}(t) dt$ is the energy received by the SiPM during the transmission of the k th sample between t_k and $t_k + T_s$. α_{PDE} is the photon detection efficiency (PDE). E_p is the energy of a single photon.

B. INVERSE CDF METHOD

In the simulation, the time interval between two adjacent arriving photons is modelled using an exponential distribution so that the number of arriving photons within a constant time period obeys the Poisson distribution in (1). The probability density function (PDF) of the exponential distribution is given by

$$p(t) = \lambda e^{-\lambda t} \quad (3)$$

where λ is the rate parameter and is related to μ_k and T_s by

$$\lambda = \frac{\mu_k}{T_s} \quad (4)$$

In the following simulation and analysis, an inverse CDF method is used to simulate the random arriving time of each photon which follows the PDF of $p(t)$. First, the CDF of (3) is calculated using

$$\begin{aligned} F_T(t) &= P(T \leq t) = \int_0^t \lambda e^{-\lambda x} dx \\ &= 1 - e^{-\frac{\mu_k}{T_s} t} \end{aligned} \quad (5)$$

The inverse CDF is then obtained using

$$t = F^{-1}(u) = -\frac{T_s}{\mu_k} \ln(1 - u) \quad (6)$$

Using the inverse CDF method, when u is a uniformly distributed random variable within 0 and 1, $u \sim U(0, 1)$, the random variable obtained, t , based on the relationship in (6) has a PDF of $p(t)$. Therefore, t is used to simulate the arrival time of individual photons and the overall number of arriving photons thus follows the Poisson

TABLE 2. The pseudo-code of the photon counting simulation process.

Input: τ, T_s
Output: $\mathbf{T}_{\text{missed}}, \mathbf{T}_{\text{detected}}$
1: $t_0 \leftarrow T_{\text{detected, initial}}$
2: $i \leftarrow 0$
3: while $t_i < T_s$ do
4: $i \leftarrow i + 1$
5: Generate $u_i \sim U(0, 1)$
6: $t_i \leftarrow t_{i-1} - \frac{T_s}{\mu_k} \ln(1 - u_i)$
7: if $t_i - T_{\text{detected}} \leq \tau$ then
8: $T_{\text{missed}} \leftarrow t_i$
9: $\mathbf{T}_{\text{missed}} \leftarrow [\mathbf{T}_{\text{missed}}, T_{\text{missed}}]$
10: else if $t_i - T_{\text{detected}} > \tau$ then
11: $T_{\text{detected}} \leftarrow t_i$
12: $\mathbf{T}_{\text{detected}} \leftarrow [\mathbf{T}_{\text{detected}}, T_{\text{detected}}]$
13: end if
14: end while

distribution in (1). The advantage of this method is that it is based on the uniformly distributed random numbers and therefore its use is not limited to simulation software programs which contain high-level statistics toolboxes or libraries.

C. SIMULATION OF THE RECOVERY TIME

As explained in the previous section, a microcell becomes inactive for a period of time after it detects a single photon. The duration of this period is known as the recovery time of the microcell, τ . It affects both the number of detected photons and its statistical properties [22]. Table-2 shows the simplified pseudo-code which is used to simulate the number of detected photons with the influence of the recovery time. In Table-2, $\mathbf{T}_{\text{missed}}$ is a vector which contains the arrival time of the photons that are undetected or missed due to the microcell's recovery time. $\mathbf{T}_{\text{detected}}$ contains the time of the detected photons and therefore the number of detected photons within a sampling period of T_s is the vector length of $\mathbf{T}_{\text{detected}}$.

IV. NONLINEARITY AND INTERFERENCE

In this section, using the simulation model described in Section-III, the origin of the SiPM's nonlinearity and the associated interference at high data rate scenarios are explained in detail.

A. THE NONLINEARITY AND ITS ORIGIN

To illustrate how the recovery time of the microcell causes a nonlinear response when the SiPM receivers are used to detect a constant light intensity, simulation trails of a single microcell are first presented to explain the photon counting process and the simulated nonlinearities of both the SiPM 30035 and the SiPM 60035 are then discussed.

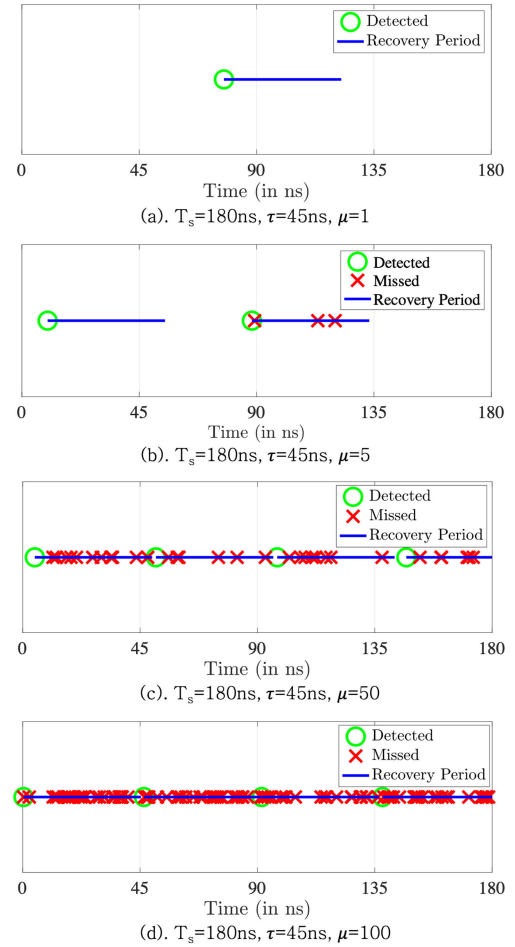


FIGURE 1. Simulations of photons that are detected and missed by a single microcell, with a recovery time of 45 ns, within a period of 180 ns. The average numbers of arriving photons within this period are (a). $\mu = 1$, (b). $\mu = 5$, (c). $\mu = 50$, (d). $\mu = 100$. In this figure, the green circles denote the detected photons, the red crosses indicate the missed photons due to the recovery time and the blue lines represent the durations of the recovery time.

Fig. 1 shows four simulation trials with different average numbers of photons arriving ($\mu = 1, \mu = 5, \mu = 50, \mu = 100$) within a sampling period of 180 ns when the recovery time is 45 ns. In Fig. 1 (a), it can be seen that only one photon arrives within the sampling period and thus all photons are detected. However, as shown in Fig. 1 (b), when the average number of arriving photons is five, only two photons are detected because the other photons arrived within the microcell's recovery period and were therefore missed. Note that, even by fixing μ at a certain value, the number of arriving photons as well as the number of detected photons vary in different trials due to the statistical features of the photon arrival times. Next, when the average number of arriving photons is further increased to 50 as shown in Fig. 1 (c), the number of detected photons is only increased to four and most of the photons are missing. Since the sampling period in these trials, 180 ns, is four times the recovery time, 45 ns, this is the maximum number of photons that can be detected in the sampling period. Hence, when the average number

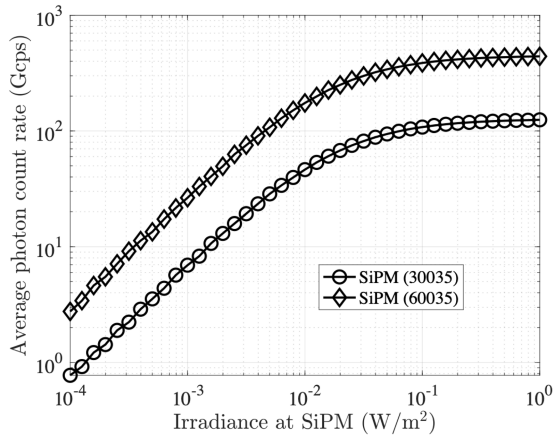


FIGURE 2. The simulated average photon detection rate (in Gcps) as a function of the irradiance falling on the SiPMs.

of arriving photons becomes 100 as shown in Fig. 1 (d), the number of detected photons remains four, which means that the microcell response is saturated.

It can be seen from Fig. 1 that, due to the recovery time of the microcell, many arriving photons are missing and thus the number of detected photons is not linearly related to the received light intensity. Fortunately, this problem can be reduced by using SiPMs which contain an array of microcells so that when some of the microcells are affected by their recovery time others are still available for detecting the arriving photons. However, the whole SiPM would eventually become saturated when the received light intensity is too high.

Next, the nonlinearity of both SiPM 30035 and SiPM 60035 are simulated and analyzed based on the parameters in Table-1. In Fig. 2, the simulated average photon detection rate is plotted as a function of the irradiance level. When the SiPM 30035 is considered, it can be seen the photon detection rate is proportional to the optical power falling on the SiPM surface when the irradiance level is up to 30 mW/m². This relationship then becomes nonlinear when the irradiance level is between 30 mW/m² and 300 mW/m². The receiver eventually becomes saturated when the irradiance is above 300 mW/m². Because SiPMs are non-paralyzable detectors and the maximum number count rate can be obtained using

$$C_{\max} = \frac{N_{\text{cells}}}{\tau} \quad (7)$$

When the parameters of SiPM 30035 in Table-1 are used, C_{\max} is 126 Gcps and it is consistent with the results shown in Fig. 2. It also can be seen that, when SiPM 60035 is considered the larger number of microcells increases the maximum count rate to 445 Gcps. This means that the SiPM 60035 can support signals with a higher dynamic range than the SiPM 30035. This higher dynamic range will reduce the distortion of signal samples with high instantaneous optical power introduced by the nonlinearities shown in Fig. 2. When the symbol period is longer than 3 ns the SiPM 60035 is therefore expected to be a better receiver than the SiPM 30035.

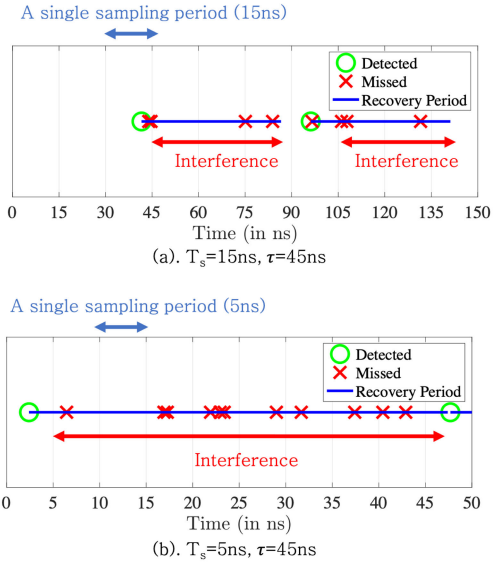


FIGURE 3. Simulations to illustrate interference between different signal samples due to the influence of the microcell's recovery time, $\tau = 45$ ns, when (a). $T_s = 15$ ns, (b). $T_s = 5$ ns.

B. INTERFERENCE BETWEEN SIGNAL SAMPLES

The non-linear response in Fig. 2 assumes that the light intensity is constant. When the irradiance falling on the SiPM varies, the recovery time of the microcells can also cause interference between different signal samples. In the examples shown in Fig. 1, the sampling period is set to be much greater than the recovery time of the microcell (e.g. 180 ns > 45 ns). In this case, the nonlinearity of the receiver predominantly affects the number of detected photons within a single sampling period when the received light intensity is high. However, to increase the data rate, the sampling period should be as short as possible. Once it is approximately the same duration as, or shorter than, the recovery period, the recovery period can cause a new type of ISI. This is because, during the detection of each transmitted signal sample, some of the microcells are inactive due to the influence of the microcell's recovery initiated during a previous sampling period. This affects the number of detected photons and causes interference between different signal samples. When the recovery time of the microcell is τ and the duration of a signal sample is T_s , the number of affected signal samples due to the recovery period of a microcell after a single photon detection is

$$L_{\text{ISI}} = \frac{\tau}{T_s} \quad (8)$$

In other words, the detection of one signal sample is affected by the detection of the previous L_{ISI} samples due to the recovery time.

To illustrate interference between different signal samples caused by the microcell recovery time Fig. 3 shows two simulation trials when the microcell's recovery time is fixed at 45 ns and the sampling periods are 15 ns and 5 ns. In these two simulation trials, the number of photons arriving within each sampling period follows a Poisson distribution and the average number of arriving photons is one. It can be seen that

the recovery period which follows a single photon detection not only affect its own sampling period but also spans over L_{ISI} sampling periods. In the example shown in Fig. 3 (a), when the sampling period is 15 ns, the recovery period affects the photon detection for three sampling periods. When the sampling period is reduced to 5 ns as shown in Fig. 3 (b), the recovery period affects nine sampling periods. These results are also consistent with (8).

V. PRE-EQUALIZATION METHOD

In this section, a new pre-equalization method, which is specially designed to mitigate the ISI caused by the recovery time described in Section-IV, is introduced. In this method, the amplitudes of the transmitted signal samples are pre-amplified based on the estimated number of active microcells. Ideally, this means that the number of photons detected within each sampling period is not affected by the recovery time of the microcells. When the number of detected photons during the transmission of the i^{th} signal sample is $N_{\text{photon}}(i)$, $N_{\text{photon}}(i)$ microcells become inactive and will not be available for photon detection in the next L_{ISI} sampling periods. Therefore, the number of inactive microcells during the detection of the n^{th} time domain signal sample depends on the overall number of detected photons in the previous L_{ISI} sampling periods and is given by

$$N_{\text{inactive}}(n) = \sum_{i=n-L_{\text{ISI}}}^{n-1} N_{\text{photon}}(i) \quad (9)$$

Thus, a ratio of the inactive number of microcells is obtained by

$$\alpha_{\text{inactive}}(n) = \frac{N_{\text{inactive}}(n)}{N_{\text{cells}}} \quad (10)$$

The ratio of the active microcells then becomes

$$\alpha_{\text{active}}(n) = 1 - \alpha_{\text{inactive}}(n) \quad (11)$$

When the number of active microcells is less than N_{cells} , the photons incident on the inactive microcells will not be detected and the overall number of detected photons is thus reduced. In order to compensate for this negative influence, the amplitude of the transmitted signal sample, $s(n)$, is pre-amplified using

$$\bar{s}(n) = \frac{s(n)}{\alpha_{\text{active}}(n)} \quad (12)$$

For example, when only half of the microcells are available, in order to detect the desired number of photons, the amplitude of the signal sample or the instantaneous optical power should be doubled.

With pre-equalization, during the transmission of the n^{th} signal sample, the received instantaneous optical power becomes

$$r_{\text{opt}}(n) = \bar{s}(n)\beta_{\text{EO}}h_0 \quad (13)$$

where β_{EO} is the electrical-to-optical conversion coefficient of the transmitter, h_0 is the optical channel gain. Both β_{EO}

and h_0 are assumed to be pre-estimated and known to the transmitter. Because only $\alpha_{\text{active}}N_{\text{cells}}$ microcells are active and the photons falls on the inactive microcells cannot be detected, the effective received optical power is therefore $\alpha_{\text{active}}r_{\text{opt}}(n)$. The estimated number of detected photons during the n^{th} period can then be obtained using

$$\begin{aligned} N_{\text{photon}}(n) &= \frac{\alpha_{\text{active}}(n)r_{\text{opt}}(n)\alpha_{\text{PDE}}T_s}{E_p} \\ &= \frac{\alpha_{\text{active}}(n)\bar{s}(n)\beta_{\text{EO}}h_0\alpha_{\text{PDE}}T_s}{E_p} \end{aligned} \quad (14)$$

It can be seen that substituting (12) in (14) gives

$$N_{\text{photon}}(n) = \frac{s(n)\beta_{\text{EO}}\alpha_{\text{PDE}}h_0T_s}{E_p} \quad (15)$$

This equation shows that, by using this signal pre-equalization step, the average number of detected photons is linearly related to the signal sample, $s(n)$. Finally, $N_{\text{photon}}(n)$ is used to calculate the number of inactive microcells in the next $(n+1)^{\text{th}}$ symbol time.

In this pre-equalization method, the ideal situation is that the number of overall microcells is sufficient to support the pre-equalization process. However, because the overall number of microcells is limited to N_{cells} and it is possible for all the microcells to become inactive. Increasing the instantaneous optical power would then no longer increase the number of detected photons. This happens when the transmitted instantaneous optical power is above

$$s_{\text{max}} = \frac{N_{\text{cells}}E_p}{\alpha_{\text{PDE}}T_s\beta_{\text{EO}}h_0}, \quad (16)$$

Taking this fact into account, the equalized signal becomes

$$\bar{s}(n) = \begin{cases} \bar{s}(n), & \text{if } \bar{s}(n) \leq s_{\text{max}} \\ s_{\text{max}}, & \text{otherwise} \end{cases} \quad (17)$$

With some rearrangement, based on (12), (15) and (16), it can be shown that the signal threshold defined in (16) is equivalent to

$$N_{\text{photon}}(n) = \alpha_{\text{active}}(n)N_{\text{cells}} \quad (18)$$

This is because, when the desired number of detected photons is greater than the number of available microcells, e.g. $N_{\text{photon}}(n) > \alpha_{\text{active}}(n)N_{\text{cells}}$, increasing the instantaneous power of the transmitted signal would not increase the number of detected photons due to the limited number of microcells. This suggests, even with pre-equalization, the number of microcells within a SiPM is a very important parameter and affects the overall system performance, especially when the irradiance level is high.

VI. SYSTEM DESCRIPTION

In this section, the transceiver structure of a VLC system using a SiPM receiver and OFDM, whose block diagram shown in Fig. 4, is described. At the transmitter, $\mathbf{X} = [X_0, X_1, \dots, X_{N-1}]$ is a bipolar complex vector representing the QAM modulated data. This is input into an IFFT where

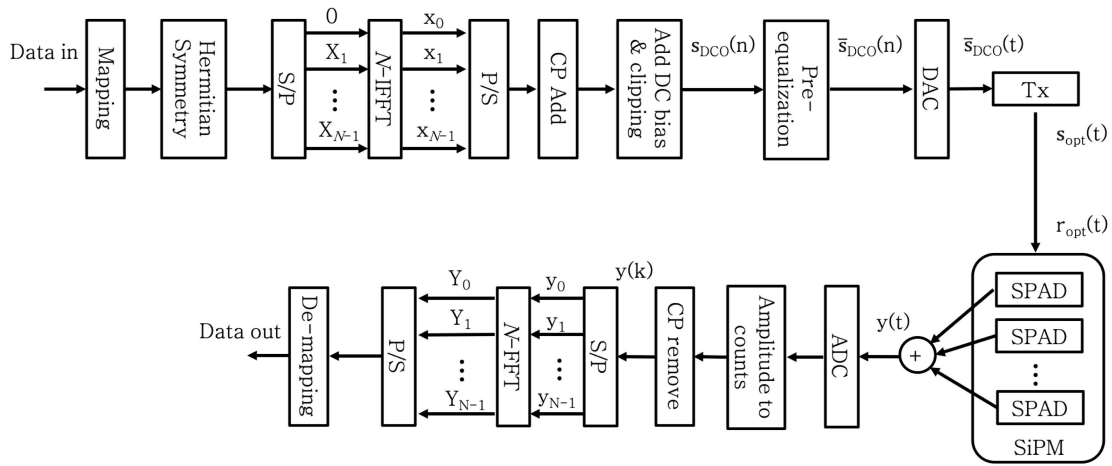


FIGURE 4. A block diagram of a system that employs OFDM, a SiPM receiver and pre-equalization.

N is the IFFT/FFT size. \mathbf{X} is constrained to have Hermitian symmetry (i.e. $X_k = X_{N-k}^*$ for $0 < k < N/2$) so that the time domain sequence, $\mathbf{x} = [x_0, x_1, \dots, x_{N-1}]$, only contains real numbers. Next, a cyclic prefix (CP) and a DC bias are added and the negative part of the signal is clipped so that the signal, $s_{\text{DCO}}(n)$, becomes unipolar. Then, this signal is pre-equalized using the method described in Section-V to generate, $\bar{s}_{\text{DCO}}(n)$. Finally, $\bar{s}_{\text{DCO}}(n)$ is sent into a DAC to obtain $\bar{s}_{\text{DCO}}(t)$ which is used to drive the transmitter. The emitted optical intensity signal, $s_{\text{opt}}(t) = \beta_{\text{EO}} \bar{s}_{\text{DCO}}(t)$, passes through an optical channel, h_{O} , before arriving at the SiPM receiver.

At the receiver, a SiPM containing N_{cells} microcells is used to detect the light intensity, $r_{\text{opt}}(t)$. The generated signal pulses from all microcells are added together via a common output. This output signal, $y(t)$, is sent into an ADC with a sampling rate of $1/T_s$. The discrete signal sequence at the output of the ADC is then converted to the number of detected photons. Next, the CP is removed and the photon counts vector obtained during a period of NT_s , $\mathbf{y} = [y_0, y_1, \dots, y_{N-1}]$, is sent into an FFT block to give $\mathbf{Y} = [Y_0, Y_1, \dots, Y_{N-1}]$ which is finally converted to a binary data sequence based on the maximum likelihood (ML) criterion.

VII. SIMULATION RESULTS

In this section, the simulation results are presented. The choices of the dc bias level and the QAM constellations are first discussed. Then, BER results are used to demonstrate the effectiveness of the new pre-equalization algorithm and also investigate the performance of the system in the presence of ambient light emitted from phosphor coated white LEDs.

A. DATA RATE

In this article, DC-biased optical OFDM (DCO-OFDM) is considered as the modulation method with the related simulation parameters shown in Table-3. In DCO-OFDM, each received symbol consists of $N + N_{\text{CP}}$ signal samples. N is

TABLE 3. OFDM Parameters.

Parameters	Value
Modulation	DCO-OFDM
Constellation size, M	4, 8, 16-QAM
Number of subcarriers, N	256
DC bias, B_{DC}	5 - 10 dB
CP length, N_{CP}	16

the FFT size and N_{CP} is the CP length. If a single sampling period is T_s , the duration of one OFDM symbol is therefore $(N + N_{\text{CP}})T_s$. The data rate of DCO-OFDM can be calculated using

$$b = \frac{\left(\frac{N}{2} - 1\right) \log_2(M)}{(N + N_{\text{CP}})T_s} \quad (19)$$

B. THE CHOICE OF DC BIAS

It has been shown in [13] that the performance of DCO-OFDM is related to the DC bias added to the signal. In this section, the optimum choice of the DC bias is discussed. In Fig. 5, the simulated BER is plotted as a function of the irradiance by considering different DC bias levels when no equalization is used. First, it shows that when the irradiance level is increased from 10^{-4} W/m^2 to 10^{-1} W/m^2 , the simulated BER first decreases and then increases for all cases. This is because, when the irradiance level is too low, the dynamic range and the variance of the photon counting signal are very small which results in high BERs. However, when the irradiance level is too high, the SiPM becomes saturated, which also degrades the overall performance. The lowest BERs are associated with the irradiance levels between 10^{-3} W/m^2 and 10^{-2} W/m^2 . When the irradiance level is within this range, the simulated BER first decreases and then increases when the DC bias is increased from 5 dB to 10 dB.

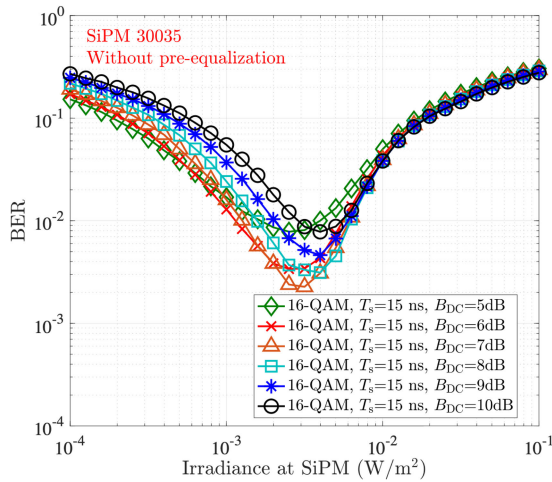


FIGURE 5. The performance of a system which employs 16-QAM and a SiPM receiver but not equalization at various dc bias levels.

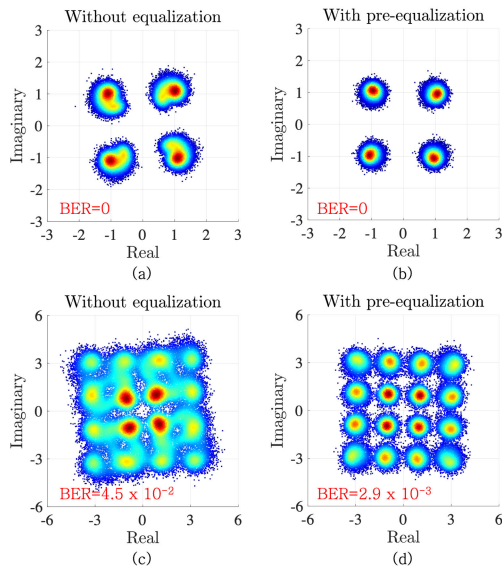


FIGURE 6. The received QAM constellations when a SiPM 30035 is used with a sampling period is 15 ns and an irradiance level is 10 mW/m², (a). 4-QAM without equalization, (b). 4-QAM with pre-equalization, (c). 16-QAM without equalization, (d). 16-QAM with pre-equalization.

This is because when the DC bias is too low the clipping distortion dominates the overall performance. However, when the DC bias is too high, the OFDM signal is affected by the nonlinear response of the SiPMs. Consequently, the best performance is achieved with a DC bias of approximately 7 dB which is therefore used in the following simulations.

C. RECEIVED QAM CONSTELLATIONS

In this section, the performance of the new pre-equalization method is studied by investigating the received QAM constellations. Two conventional forms of square QAM constellations, 4-QAM and 16-QAM, are first considered. Fig. 6 shows the received QAM constellations with and without using pre-equalization when the parameters of the SiPM 30035 are used in the simulation. It can be seen from

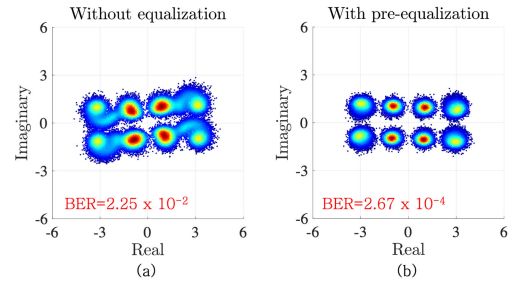


FIGURE 7. The received QAM constellations when a SiPM 30035 is used with a sampling period of 15 ns and an irradiance level is 10 mW/m² (a). 8-QAM without pre-equalization, (b). 8-QAM with pre-equalization.

Fig. 6 (a) and Fig. 6 (c) that the signal distortion is significant when no equalization is used. In the specific examples considered in Fig. 6, the 4-QAM case has a BER of 0 and the 16-QAM case has a BER of 4.5×10^{-2} . When the pre-equalization method is used, the BER of 4-QAM remains 0 and the BER of 16-QAM is reduced to 2.9×10^{-3} . The benefits of using the pre-equalization method can be clearly seen from these constellations.

Although the pre-equalization can significantly reduce the BERs, it can be observed from Fig. 6 (d) that, the four ‘corners’ of the constellation are more scattered than the other parts of the constellation. Taking this into account, the performance of a specific form of 8-QAM shown in Fig. 7 is also studied. Fig. 7 shows that the BER is 2.25×10^{-2} without using equalization and then reduced to 2.67×10^{-4} using pre-equalization. Compared to the 16-QAM case in Fig. 6 (d), the BER is reduced by a factor of almost 10 in Fig. 7 (b). If the forward error correction (FEC) limit is set to be 10^{-3} [23], 8-QAM provides the best performance since the achieved data rate is higher than 4-QAM and the BER is lower than 16-QAM. If the 7 % FEC limit which is 3.8×10^{-3} is considered [24]–[26], 16-QAM becomes the best option in this case.

D. BER RESULTS OF SiPM 30035

Fig. 8 shows the simulated BER results with and without using the pre-equalization method when SiPM 30035 is considered. It can be seen that, when the irradiance level is low, equalization has a small impact on BER. This is because the average number of detected photons is extremely small when the irradiance level is below 10^{-3} W/m² and almost no photons arrive within the recovery time of the microcells. Therefore, the interference between different signal samples is very low and hence the pre-equalization has little effect. However, when the irradiance level becomes higher, both the number of detecting photons and the number of missed photons increase and, as shown in Fig. 8, the pre-equalization method can significantly reduce the BER. If the FEC limit is set to be 10^{-3} , it can be seen that when no equalization is used 4-QAM supports the highest data rate which is 187 Mbit/s. When the pre-equalization method is used, 8-QAM becomes the best option and the highest data rate is increased to 280 Mbit/s as shown in Fig. 8 (b). If the FEC

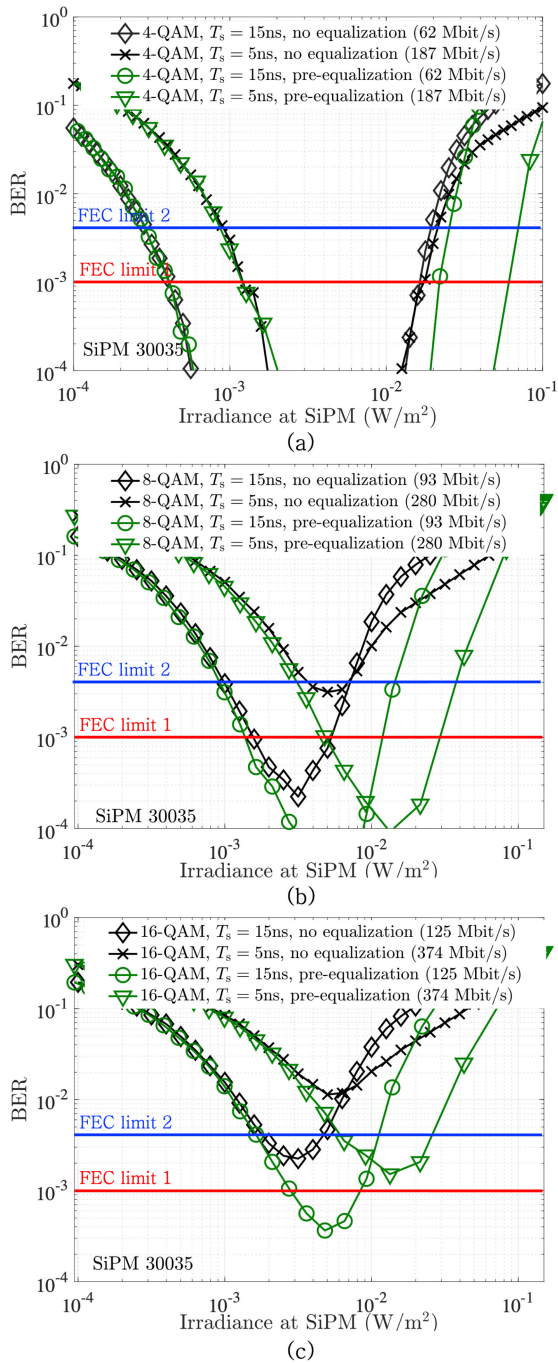


FIGURE 8. Simulated BER as a function of the irradiance level with and without equalization using a SiPM 30035 (a). 4-QAM, (b). 8-QAM, (c). 16-QAM.

limit is considered to be 3.8×10^{-3} , the 8-QAM supports the highest data rate of 280 Mbit/s when no equalization is used and 16-QAM supports the highest data rate of 374 Mbit/s with pre-equalization.

E. BER RESULTS OF SiPM 60035

As shown in Fig. 2, the dynamic range of the photon counting signal can be increased by using a SiPM with more

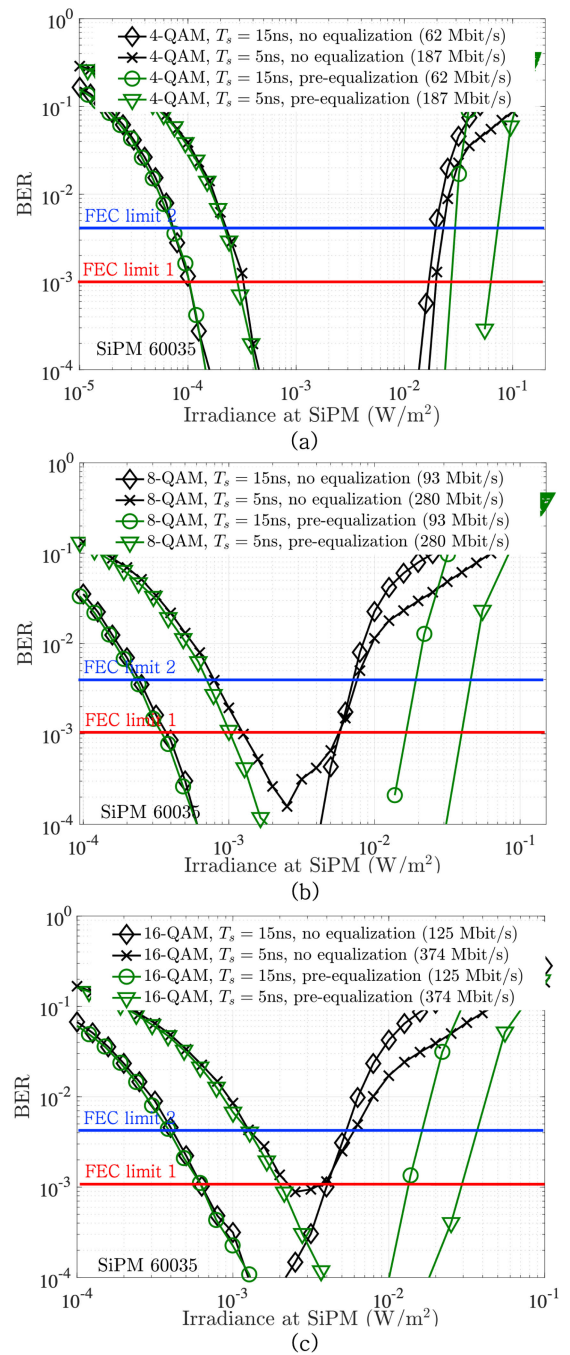


FIGURE 9. Simulated BER as a function of the irradiance level with and without equalization using a SiPM 60035 (a). 4-QAM, (b). 8-QAM, (c). 16-QAM.

microcells. More importantly, the threshold defined in (16) indicates that the performance of the pre-equalization method is affected by N_{cells} . In this section, the BER results of SiPM 60035 are analyzed and compared to those of SiPM 30035. First, it can be seen from Fig. 9 that, for both FEC limits (10^{-3} or 3.8×10^{-3}), the achievable data rate is always 374 Mbit/s when 16-QAM is used. Next, in order to compare the BER performance of the SiPM 60035 and SiPM 30035 their BER results are shown in the same figure

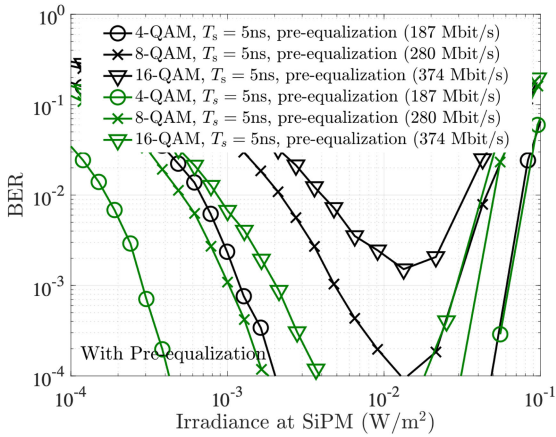


FIGURE 10. A comparison of the BER performance of the SiPM 30035 and SiPM 60035 with different constellations.

in Fig. 10. It can be seen that, regardless of the irradiance level and the constellation size, the BERs obtained using the SiPM 60035 are much lower than those obtained using the SiPM 30035. This is because, when the irradiance levels are low, the signal detected by the SiPM 60035 has a higher dynamic range which results in lower BERs. When the irradiance levels are high and the nonlinearity of the SiPM causes interference, but, the pre-equalization method is more effective when used with the SiPM 60035.

F. THE INFLUENCE OF THE BACKGROUND COUNTS

As shown in the previous sections that the SiPM 60035 has a better performance than the SiPM 30035 and in particular, it can support the constellation of 16-QAM and a short sampling period of 5 ns. In this section, the performance of this configuration is further investigated by including the influence of the background counts which are mainly caused by the ambient light that will be present when a VLC system is deployed. When the background photons are considered, the BER performance is related to both the number of photons arriving at the SiPM from the transmitter and the number of detected photons from the ambient light.

Ambient light is expected to have a significant impact when the number of photons of ambient light that are detected is comparable to the number of detected photons from the transmitter. As shown in previous figures, the lowest BER occurs when the irradiance from the transmitter is 10^{-2} W/m². The histogram of the average number of detected photons, μ_{signal} , within each 5 ns sampling period for an ideal, linear channel is shown in Fig. 11. It can be seen that the photons number ranges from 0 to 4000 and also follows a clipped Gaussian distribution [13].

Based upon the distribution in Fig. 11 the BER was simulated for a range of different average numbers of background counts, $\mu_{\text{background}}$, including $\mu_{\text{background}} = 200$, $\mu_{\text{background}} = 500$, $\mu_{\text{background}} = 1000$, $\mu_{\text{background}} = 1500$, $\mu_{\text{background}} = 2000$. These chosen values are also marked in Fig. 11 so that they can be easily compared to the signal photon numbers. The simulated BER results are shown

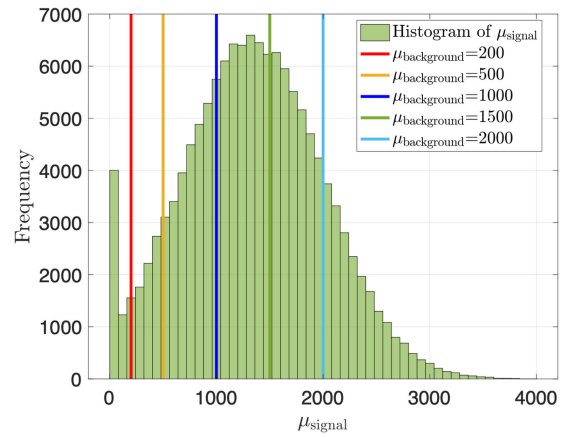


FIGURE 11. The histogram of the average number of photons due to the received DCO-OFDM signal when the irradiance level is 10^{-2} W/m².

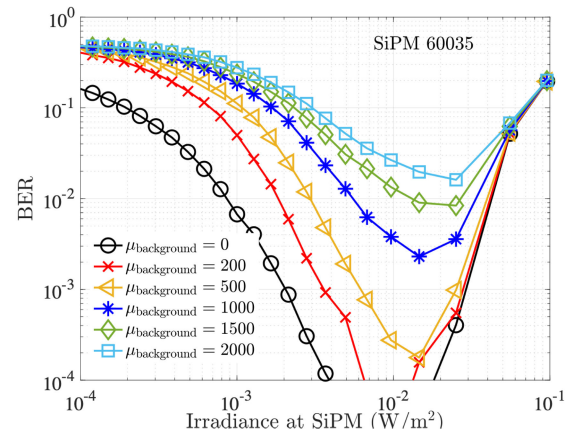


FIGURE 12. The BER plots with different average numbers of background counts using SiPM 60035 with 16-QAM and $T_s=5$ ns.

in Fig. 12. These results show that, when $\mu_{\text{background}}$ is less than 1000, its influence on the BER is relatively small and the BER remains low for a wide range of irradiance levels. However, when $\mu_{\text{background}}$ is greater than 1500, the BERs are all above the FEC limit.

In order to maintain the systems performance, optical filters will be required which limit the number of ambient light photons that are detected by the SiPM to less than 1500 in 5 ns. The impact of the spectrum and intensity of the ambient light on the rate at which ambient light photons are detected has therefore been investigated. (The detailed calculation of this relationship is provided in the Appendix.) In this study, it was assumed that the ambient light is emitted from a phosphor-coated white LED. The two popular types of white LEDs considered where the ‘warm’ LED (3000 K) and the ‘cool’ LED (5000 K) and their normalized output spectra are shown in Fig. 13. In Fig. 14, the ambient light level (in lux) is plotted as a function of the associated background photons without placing optical filters in the front of the SiPM. First, it can be seen that the cool white LED results in more detected photons than the warm white LED. This is because, compared to the warm white LED, the light emitted from the cool white

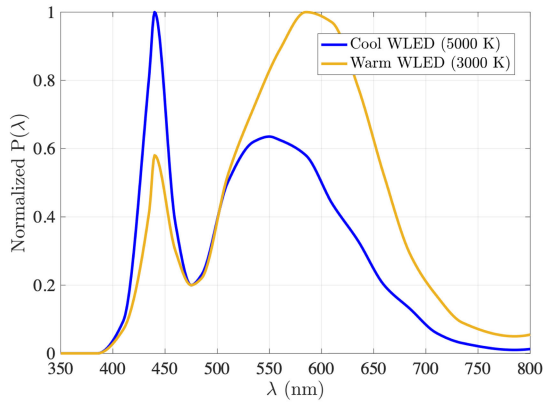


FIGURE 13. Output optical spectra of two phosphor based white LEDs.

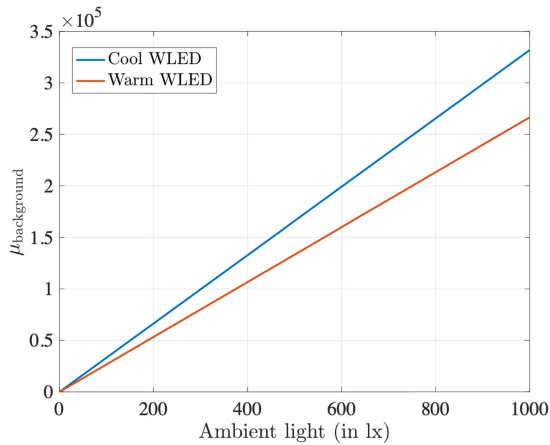


FIGURE 14. The number of background counts due to the ambient light at different illumination levels of two different types of white LEDs.

LED has more power between 400 nm and 500 nm and the SiPM's PDE coefficients are also large within this range as shown in Fig. 16. Next, as shown in Fig. 14, if the SiPM was a linear device, in 500 lux of ambient light approximately 1.5×10^5 ambient light photons would be detected in 5 ns. Together with the BER results shown in Fig. 12, this suggests that an optical filter is required to remove 99 % of these photons so that less than 1500 ambient light photons are detected in 5 ns. If this isn't possible the maximum data rate that can be supported will be reduced.

VIII. CONCLUSION

In this article, Monte Carlo simulations were used to show how the finite recovery time of microcells in a SiPM cause both a nonlinear response and a new form of inter-symbol interference. A new time domain based pre-equalization method, which is specially designed to reduce the impact of the recovery time caused ISI was then described and studied. The results that were presented show that the BER performance of the system can be significantly improved by pre-adjusting the amplitudes of the transmitted signal samples based on the estimated fraction of microcells that are active. When optical OFDM is used as the modulation

method, the BER performance of both the SiPM 30035 and SiPM 60035 was investigated. The results from the simulations of the SiPM 30035 show that without equalization 4-QAM supports the highest data rate. When the new pre-equalization method is used, a special form of non-square 8-QAM becomes the best option and the transmission data rate can be increased to 280 Mbps with the BER level below 10^{-3} for a wide range of irradiance levels. Other results showed that the performance of the system can be further enhanced by increasing the number of microcells within the SiPM. In particular when a SiPM 60035 is considered. With this SiPM 16-QAM is a better than both 4-QAM and 8-QAM. Consequently, the results predict that a data rate of 374 Mbits/s can be achieved over a wide range of irradiance levels. This data rate is much higher than any previously predicted data when OFDM modulation and a receiver based upon a SiPM or an array of SPADs are used. Finally, an investigation of the influence of background counts from ambient light suggests that to maintain this data rate filters will be required which reduce the detected background count rate by 99%.

Some future work will focus upon identifying the wide field of view optical filters needed to significantly reduce the impact of ambient light on the SiPM receiver. In addition, the data rates that can be achieved by combining OFDM and a SiPM receiver should be investigated by building and testing a SiPM receiver specifically designed to support OFDM. Initially this system should be used to confirm the simulation results that have been reported. Once these experiments have been completed the effectiveness of using pre-equalization to compensate from recovery time induced ISI and post-equalization to compensate for ISI created by the limited bandwidth of the channel should be confirmed. Using these complementary forms of equalization data rates of more than 1 Gbps should be achievable.

APPENDIX

THE BACKGROUND PHOTON COUNTS AND AMBIENT LIGHT

In this Appendix, the relationship between the ambient light intensity and its associated background photon counts is analyzed. In most of the indoor environment, the illumination level (or illuminance), E_v , usually ranges from 100 lux to 1000 lux for normal daily activities and it is related to luminous flux (in lm), Φ_v , by

$$\Phi_v = E_v A \quad (20)$$

where A is the illumination area which is considered to be the area of the SiPM detector in this case. The relationship between the illumination level and the related optical power, $P_{\text{ambient,opt}}$, is given by

$$\Phi_v = 683 \text{ lm/W} \times \int_{\lambda} P_{\text{ambient,opt}} P(\lambda) V(\lambda) d\lambda \quad (21)$$

where $V(\lambda)$ is the normalized luminous efficiency, shown in Fig. 15, which has a maximum value of 683 lm/W and

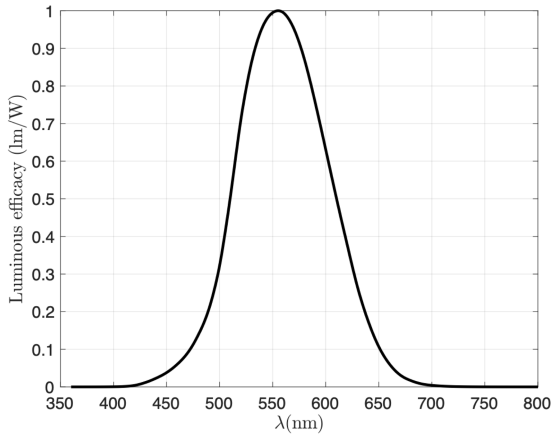


FIGURE 15. The normalized luminous efficiency for different wavelengths.

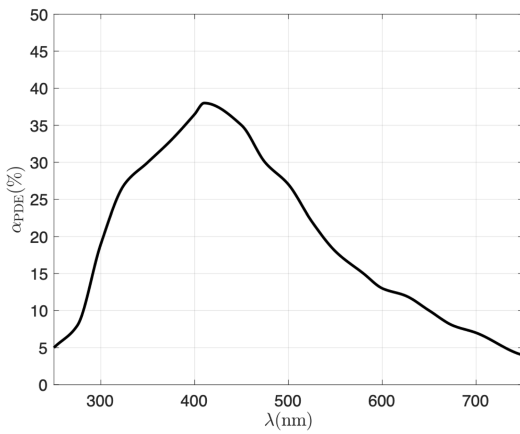


FIGURE 16. The photon detection efficiency (PDE) for different wavelengths at an over-voltage of 2.5 V. The data used to create this figure was obtained from a figure in [21].

peaks at approximately 555 nm. $P(\lambda)$ is the optical spectrum of the light source. Note that, $P(\lambda)$ used in (21) follows $\int_{\lambda} P(\lambda) d\lambda = 1$ which therefore has a different scale compared to the *normalized* coefficients shown in Fig. 13. Based on (20) and (21), the relationship between the received optical power and the illumination level is given by

$$P_{\text{ambient,opt}} = \frac{E_v A}{683 \text{ lm/W} \times \int_{\lambda} P(\lambda) V(\lambda) d\lambda} \quad (22)$$

Next, the average number of photons arriving at the SiPM due to the ambient light can be calculated using

$$\mu_{\text{background}} = P_{\text{ambient,opt}} T_s \int_{\lambda} \frac{P(\lambda) \alpha_{\text{PDE}}(\lambda)}{E_p(\lambda)} d\lambda \quad (23)$$

where

$$E_p(\lambda) = \frac{hc}{\lambda} \quad (24)$$

is the energy of a single photon which has a wavelength of λ , h is the Planck constant, c is the speed of light in vacuum. $\alpha_{\text{PDE}}(\lambda)$ is the photon detection efficiency (PDE) of the SiPM detector which also depends on wavelength. Some values for

PDE at different wavelengths have been extracted from a figure in [21]. Interpolation was then used to create the results shown in Fig. 16, which were used in (23).

REFERENCES

- [1] T. Komine and M. Nakagawa, "Fundamental analysis for visible-light communication system using LED lights," *IEEE Trans. Consum. Electron.*, vol. 50, no. 1, pp. 100–107, Feb. 2004.
- [2] A. Jovicic, J. Li, and T. Richardson, "Visible light communication: Opportunities, challenges and the path to market," *IEEE Commun. Mag.*, vol. 51, no. 12, pp. 26–32, Dec. 2013.
- [3] H. Haas, L. Yin, Y. Wang, and C. Chen, "What is LiFi?" *J. Lightw. Technol.*, vol. 34, no. 6, pp. 1533–1544, Mar. 15, 2016.
- [4] F. Zafar, M. Bakaul, and R. Parthiban, "Laser-diode-based visible light communication: Toward gigabit class communication," *IEEE Commun. Mag.*, vol. 55, no. 2, pp. 144–151, Feb. 2017.
- [5] D. Karunatilaka, F. Zafar, V. Kalavally, and R. Parthiban, "LED based indoor visible light communications: State of the art," *IEEE Commun. Surveys Tuts.*, vol. 17, no. 3, pp. 1649–1678, 3rd Quart., 2015.
- [6] D. O'Brien, S. Rajbhandari, and H. Chun, "Transmitter and receiver technologies for optical wireless," *Phil. Trans. Roy. Soc. A, Math., Phys. Eng. Sci.*, vol. 378, no. 2169, Apr. 2020, Art. no. 20190182.
- [7] S. Cova, M. Ghioni, A. Lacaita, C. Samori, and F. Zappa, "Avalanche photodiodes and quenching circuits for single-photon detection," *Appl. Opt.*, vol. 35, no. 12, pp. 1956–1976, 1996.
- [8] Z. Ahmed, R. Singh, W. Ali, G. Faulkner, D. O'Brien, and S. Collins, "A SiPM-based VLC receiver for gigabit communication using OOK modulation," *IEEE Photon. Technol. Lett.*, vol. 32, no. 6, pp. 317–320, Mar. 15, 2020.
- [9] L. Zhang, H. Chun, Z. Ahmed, G. Faulkner, D. O'Brien, and S. Collins, "The future prospects for SiPM-based receivers for visible light communications," *J. Lightw. Technol.*, vol. 37, no. 17, pp. 4367–4374, Sep. 1, 2019.
- [10] W. Matthews, Z. Ahmed, W. Ali, and S. Collins, "A SiPM-based VLC receiver for 3.45 Gigabits/s communication using OOK modulation," in *Proc. IEEE Photon. Conf. (IPC)*, Sep. 2020, pp. 1–2.
- [11] L. Zhang, X. Tang, C. Sun, Z. Chen, Z. Li, H. Wang, R. Jiang, W. Shi, and A. Zhang, "Over 10 attenuation length gigabits per second underwater wireless optical communication using a silicon photomultiplier (SiPM) based receiver," *Opt. Exp.*, vol. 28, no. 17, pp. 24968–24980, 2020.
- [12] J. Armstrong, "OFDM for optical communications," *J. Lightw. Technol.*, vol. 27, no. 3, pp. 189–204, Feb. 1, 2009.
- [13] S. D. Dissanayake and J. Armstrong, "Comparison of ACO-OFDM, DCO-OFDM and ADO-OFDM in IM/DD systems," *J. Lightw. Technol.*, vol. 31, no. 7, pp. 1063–1072, Apr. 1, 2013.
- [14] T. Essalih, M. A. Khalighi, S. Hranilovic, and H. Akhouchy, "Optical OFDM for SiPM-based underwater optical wireless communication links," *Sensors*, vol. 20, no. 21, p. 6057, Oct. 2020.
- [15] Y. Li, M. Safari, R. Henderson, and H. Haas, "Optical OFDM with single-photon avalanche diode," *IEEE Photon. Technol. Lett.*, vol. 27, no. 9, pp. 943–946, May 1, 2015.
- [16] Y. Li, M. Safari, R. Henderson, and H. Haas, "Nonlinear distortion in SPAD-based optical OFDM systems," in *Proc. IEEE Globecom Workshops (GC Wkshps)*, Dec. 2015, pp. 1–6.
- [17] S. Huang and M. Safari, "Quantum limited optical receivers in the presence of intersymbol interference," in *Proc. 45th Eur. Conf. Opt. Commun. (ECOC)*, 2019, pp. 1–4.
- [18] S. Huang, S. M. Patanwala, J. Kosman, R. K. Henderson, and M. Safari, "Optimal photon counting receiver for sub-dead-time signal transmission," *J. Lightw. Technol.*, vol. 38, no. 18, pp. 5225–5235, Sep. 15, 2020.
- [19] C. He, Z. Ahmed, and S. Collins, "Optical OFDM and SiPM Receivers," in *Proc. IEEE Globecom Workshops (GC Wkshps)*, Dec. 2020, pp. 1–6.
- [20] W. Ali, G. Faulkner, Z. Ahmed, W. Matthews, D. O'Brien, and S. Collins, "SiPM receivers and future VLC systems," in *Proc. IEEE Globecom Workshops (GC Wkshps)*, Dec. 2020, pp. 1–6.
- [21] *J-SERIES SiPM: Silicon Photomultiplier Sensors, J-Series (SiPM)*. Accessed: Jan. 15, 2020. [Online]. Available: <https://www.onsemi.com/products/sensors/silicon-photomultipliers-sipm/j-series-sipm>
- [22] E. Sarbazi, M. Safari, and H. Haas, "Statistical modeling of single-photon avalanche diode receivers for optical wireless communications," *IEEE Trans. Commun.*, vol. 66, no. 9, pp. 4043–4058, Sep. 2018.
- [23] S. Dimitrov and H. Haas, *Principles of LED Light Communications: Towards Networked Li-Fi*. Cambridge, U.K.: Cambridge Univ. Press, 2015.

- [24] (2004). *Forward Error Correction for High Bit-Rate DWDM Submarine Systems*. [Online]. Available: <https://www.itu.int/rec/T-REC-G.975.1-200402-I/en>
- [25] K. Yoshida, P. P. Manousiadis, R. Bian, Z. Chen, C. Murawski, M. C. Gather, H. Haas, G. A. Turnbull, and I. D. W. Samuel, "245 MHz bandwidth organic light-emitting diodes used in a gigabit optical wireless data link," *Nature Commun.*, vol. 11, no. 1, pp. 1–7, Dec. 2020.
- [26] Y. Wang, Y. Wang, N. Chi, J. Yu, and H. Shang, "Demonstration of 575-Mb/s downlink and 225-Mb/s uplink bi-directional SCM-WDM visible light communication using RGB LED and phosphor-based LED," *Opt. Exp.*, vol. 21, no. 1, pp. 1203–1208, 2013.



CUIWEI HE received the Ph.D. degree in optical wireless communication from Monash University, Melbourne, Australia, in 2017. He has worked as a Research Fellow with Monash University, from September 2017 to April 2020. He is currently a Postdoctoral Research Assistant with the Department of Engineering Science, University of Oxford, U.K. His research interests include visible light communication, visible light positioning, optical wireless communication, multiple-input multiple-output (MIMO) technology, optical orthogonal frequency division multiplexing (OFDM), and optical receiver design.



ZUBAIR AHMED received the M.Sc. degree in communication electronics from Linköping University, Sweden, in 2013. He is currently pursuing the D.Phil. degree with the Department of Engineering Science, University of Oxford. His thesis is focused on the characterization of single-photon avalanche detectors, such as silicon photomultipliers (SiPMs) and their performance evaluation as ultra-sensitive visible light communication (VLC) receivers. He is currently continuing his research on estimating the performance of SiPM-based VLC receivers in the presence of ambient light.



STEVE COLLINS (Member, IEEE) received the Ph.D. degree in theoretical physics from The University of Warwick, Warwick, U.K., in 1986. He is currently an Associate Professor in engineering science and a Fellow of the University College Oxford. From 1985 to 1997, he has worked as the Research Scientist on various topics, including the origins of 1/f noise in MOSFETs, imaging sensors, and analogue information processing. Since 1997, he has been on the Academic Staff of the University of Oxford, Oxford, U.K. His research has focused upon light detecting sensors manufactured on silicon CMOS processes, including wide dynamic range CMOS imagers, optical communications receivers, and single photon avalanche detectors. His research interests include the design, manufacture, and testing of three different generations of wide dynamic range CMOS imagers, wide field of view optical concentrators, and photon counting receivers for optical communications. Based upon his work, he has more than ten granted patents and published more than 100 articles. He is also the Principle Investigator on a three year project (EP/R00689X/1 Super Receivers for Visible Light Communications), whose aim is to create visible light communications receivers that are 100 times more sensitive than existing receivers.

...